SurfaceVoronoi: Efficiently Computing Voronoi Diagrams Over Mesh Surfaces with Arbitrary Distance Solvers

SHIQING XIN, Shandong University, China
PENGFEI WANG, Shandong University, China
RUI XU, Shandong University, China
DONGMING YAN, National Laboratory of Pattern Recognition (NLPR), Institute of Automation, Chinese Academy of Sciences, and School of AI, University of Chinese Academy of Sciences, China
SHUANGMIN CHEN*, Qingdao University of Science and Technology, China
WENPING WANG, Texas A&M University, USA
CAIMING ZHANG, Shandong University, China
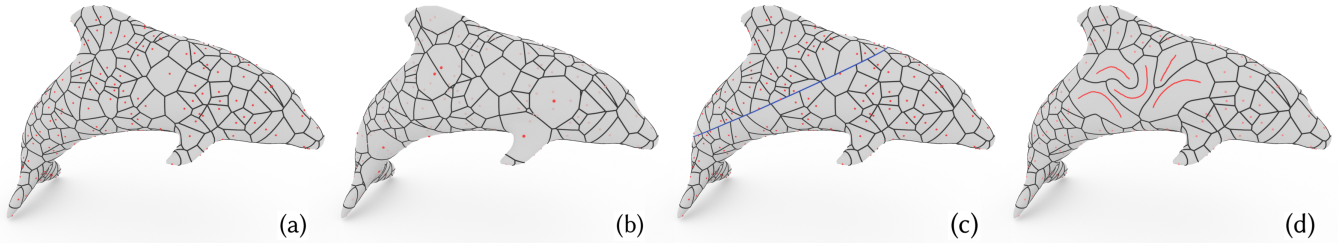CHANGHE TU, Shandong University, China

Fig. 1. We propose a novel algorithm for computing surface-based Voronoi diagrams, without the need of an off-the-shelf Voronoi/Delaunay solver. Our algorithm supports an arbitrary geodesic algorithm to drive the partition; Specially, it also supports Euclidean distance (a). Our algorithm is flexible enough to handle various versions of surface-based Voronoi diagrams. For example, it can be used to compute the surface-based power diagram (b). Furthermore, it enables users to draw breaklines to prevent any Voronoi cell from crossing the breaklines (c), and naturally supports curve segments as the source sites (d).

In this paper, we propose to compute Voronoi diagrams over mesh surfaces driven by an arbitrary geodesic distance solver, assuming that the input is a triangle mesh as well as a collection of sites $P = \{p_i\}_{i=1}^{m}$ on the surface. We propose two key techniques to solve this problem. First, as the partition is determined by minimizing the m distance fields, each of which rooted at a source site, we suggest keeping one or more distance triples, for each triangle, that may help determine the Voronoi bisectors when one uses a mark-and-sweep geodesic algorithm to predict the multi-source distance field. Second, rather than keep the distance itself at a mesh vertex, we use the squared distance to characterize the linear change of distance field restricted in a triangle, which is proved to induce an exact VD when the base surface reduces to a planar triangle mesh. Specially, our algorithm also supports the Euclidean distance, which can handle thin-sheet models (e.g. leaf) and runs faster than the traditional restricted Voronoi diagram (RVD) algorithm. It is very extensible to deal with various variants of surface-based Voronoi diagrams including (1) surface-based power diagram, (2) constrained Voronoi diagram with curve-type breaklines, and (3) curve-type generators. We

conduct extensive experimental results to validate the ability to approximate the exact VD in different distance-driven scenarios.

CCS Concepts: • **Computing methodologies** → **Mesh geometry models**.

Additional Key Words and Phrases: digital geometry processing, geodesic distance, geodesic Voronoi diagram, restricted Voronoi diagram

1 INTRODUCTION

Partitioning the 2-manifold surface S into regions based on the proximity to a given set of points $P = \{p_i\}_{i=1}^{m}$ is a fundamental operation in geometry processing. Surface-based Voronoi diagram (VD) has many important applications ranging from mesh quality improvement [Lévy and Liu 2010] to surface reconstruction [Khoury and Shewchuk 2016], and can even mimic natural tessellation patterns [Zayer et al. 2018]. It can be seen as the extension of Voronoi diagram (VD) in $\mathbb{R}^2$ to the 2-manifold surface, while the difference is that geodesic distance serves as the metric to drive the computation of surface-based VDs. Although the study of VD in $\mathbb{R}^2$ is relatively mature, efficiently computing surface-based VDs is still a challenging task.

The challenges lie in several aspects. First, in the past research, the choice of geodesic algorithms [Liu et al. 2010, 2017; Wang et al. 2015] is highly coupled with designing the scheme for computing

*Shuangmin Chen is the corresponding author.

Authors' addresses: Shiqing Xin, Shandong University, China, xinshiqing@sdu.edu.cn; Pengfei Wang, Shandong University, China, pengfei1998@foxmail.com; Rui Xu, Shandong University, China, xrvitd@163.com; Dongming Yan, National Laboratory of Pattern Recognition (NLPR), Institute of Automation, Chinese Academy of Sciences, and School of AI, University of Chinese Academy of Sciences, China, yandongming@gmail.com; Shuangmin Chen, Qingdao University of Science and Technology, China, csmqq@163.com; Wenping Wang, Texas A&M University, USA, wenping@tamu.edu; Caiming Zhang, Shandong University, China, czhang@sdu.edu.cn; Changhe Tu, Shandong University, China, chtu@sdu.edu.cn.

surface-based VDs. Second, there are various versions of surface-based VDs but the known algorithms [Wang et al. 2020; Yan et al. 2009, 2013] are not flexible enough to provide an all-in-one solution. Finally, Euclidean distance is an approximate alternative to geodesic distance especially when the sites are dense enough, which accounts for why the restricted Voronoi diagram (RVD) [Yan et al. 2009] is popular in the computer graphics community. However, it is not easy to adapt RVD to deal with a thin-sheet model because there are point pairs with very small spatial distance but long geodesic distance on these models.

It is observed that the surface-based Voronoi diagram can be extracted by finding the lower envelope of the m distance fields, each one rooted at a source site. By taking the change of a single-source distance field restricted in a triangle f as linear, the surface VD in f, determined by multiple sites, can be computed by intersecting a collection of half-planes. Inspired by this observation, we propose a powerful algorithm, named *SurfaceVoronoi*, for computing surface-based Voronoi diagrams, without the need of an off-the-shelf Voronoi/Delaunay solver. The contributions are two-fold. On one hand, we adapt the user-specified mark-and-sweep geodesic algorithm such that each triangle keeps one or more distance triples that may help determine the Voronoi bisectors. Note that even if a source cannot provide the closest distance to any vertex of the triangle, it may still provide the closest distance to an area within the triangle. Therefore, for the existing multi-source geodesic algorithms [Moenning and Dodgson 2004] that only keep the closest source for each mesh vertex, it is impossible to infer the surface VD structure accurately. Additionally, rather than keep the distance itself at mesh vertices, we use the squared distance to define the linear change in a triangle, which facilitates reporting the exact VD when the curved surface reduces to a planar triangle mesh.

Our SurfaceVoronoi algorithm has many distinguished features. First, it can work with an arbitrary geodesic algorithm, and even supports the Euclidean distance as the driving measure; See Fig. 1(a). Depending on the geodesic-distance type, our algorithm can produce various kinds of diagrams including exact geodesic Voronoi diagram (EGVD), approximate geodesic Voronoi diagram (AGVD), and Euclidean distance based Voronoi diagram (EDBVD), where EDBVD can naturally handle thin-sheet models and runs faster than the traditional restricted Voronoi diagram (RVD). Second, our algorithm is flexible enough to deal with various versions of surface-based Voronoi diagrams. For example, it can be used to compute the surface-based power diagram (see Fig. 1(b)). Furthermore, it can handle the scenario where users draw some breaklines to prevent any Voronoi cell across the breaklines (see Fig. 1(c)). It even supports curve-type sites or face-interior sites (see Fig. 1(d)). Finally, it could work on a base surface equipped with a non-uniform density field.

2 RELATED WORK

2.1 VD in Euclidean spaces

Given a set of generators (also called sites) $P = \{p_i \in \mathbb{R}^d\}_{i=1}^m$, the VD defines the partition of $\mathbb{R}^d$ into convex regions (may be unbounded) based on the proximity to the generators, where the

site p_i dominates the subregion

$$\Omega_i = \{x \in \mathbb{R}^d \mid \|x - p_i\| \leq \|x - p_j\|, \ \forall j \neq i\}. \tag{1}$$

VD, as well as its dual (i.e., Delaunay triangulation), has been widely applied to many science and engineering fields [Senechal 1993], including computer graphics, image processing, robot navigation, computational chemistry, materials science, and climatology. There is a large body of literature on computing VDs in computational geometry. Some typical computing paradigms include the divide-and-conquer scheme [Shamos and Hoey 1975], incremental construction [Green and Sibson 1978], and Fortune's sweep line [Fortune 1987]. An interesting fact is that VD or Delaunay triangulation can be constructed by a lifting technique [Fortune 1995].

2.2 VD on 2-manifold surfaces

The definition of VD can be extended to a general metric space different from Euclidean spaces [Giblin and Kimia 2004]. Construction of VDs on curved surfaces, particularly non-differentiable polyhedral surfaces, is of great significance in digital geometry processing. Roughly speaking, the methods used for computing surface-based Voronoi diagrams can be categorized into three groups, including (1) operating on the mesh surface directly based on geodesic distance [Liu et al. 2010; Wang et al. 2015], (2) operating on the parametrization plane [Rong et al. 2010] and (3) operating in the 3D Euclidean space [Wang et al. 2020; Yan et al. 2014, 2009] with the help of a 3D Voronoi/Delaunay solver. Generally speaking, geodesic distance based approaches are time-consuming and coupled with the scheme for computing surface-based VDs. For example, Liu et al. [2010] studied the analytic structure of iso-contours, bisectors, and Voronoi diagrams on a triangular mesh and further proposed a geodesic Voronoi diagram (GVD) algorithm based on the window propagation scheme of MMP's algorithm [Mitchell et al. 1987]. There are some other GVD approaches that are highly coupled with the window propagation mechanism [Qin et al. 2017; Xu et al. 2014]. Parametrization-based approaches [Alliez et al. 2005; Rong et al. 2010] need to precompute a global parametrization and thus suffer from numerical issues and topological difficulties. By substituting Euclidean distances for geodesic distances, the restricted VD (RVD) [Wang et al. 2020; Yan et al. 2014, 2009] runs many times faster, but for models with thin parts, it may violate the property of "one site, one region". Only when the sites are enough and dense, can RVD be taken as an approximate alternative to GVD. Later, Yan et al. [2014] proposed localized RVD (LRVD), first inferring neighboring relationship and then partitioning the surface, to handle thin-plate models, but LRVD does not explicitly address poor triangulation quality. Wang et al. [2020] gave a fast post-processing technique for fixing the problematic RVD cells by enforcing the property of "one site, one region". Herholz et al. [2017] proposed diffusion diagrams based on heat diffusion. Their algorithm is only equivalent to back-substitution if factorization of the system matrix is done in a preprocess.

In this paper, we propose an all-in-one solution to decouple the geodesic solver from the computation of surface VDs. Furthermore, we bridge the gap between geodesic VDs and Euclidean VDs.
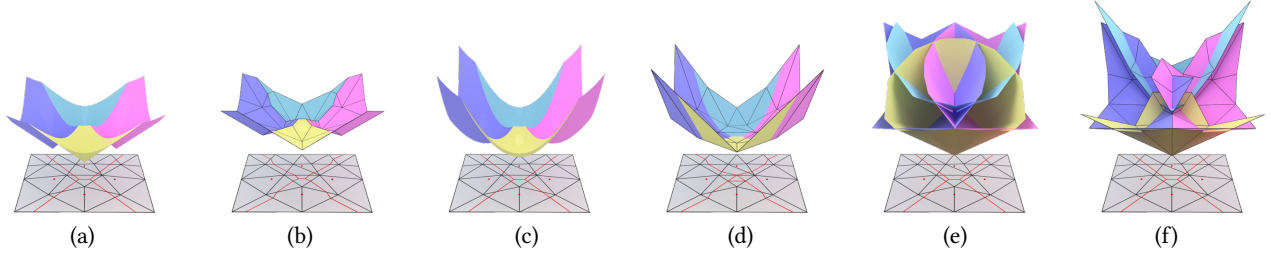
(a) (b) (c) (d) (e) (f)

Fig. 2. The VD based on lifting distance fields. (a) In 2D, the VD can be obtained by finding the lower envelope of a set of distance fields $\{D_i\}_{i=1}^{m}$, each of which is a cone rooted at a site. (b) It can be easily extended to polygonal meshes. By finding the lower envelope of m discrete distance fields, one can get an approximate VD. (c) If we use the squared distance to define a continuous parabolic surface rooted at each site, the lower envelope can also report the VD. (d) It is hard to get an accurate VD from the multi-source distance field. (e) Interestingly, the lower envelope of the m discrete squared-distance fields is able to report the exact VD when the base surface is reduced to a planar surface (we have proved the observation in this paper). (f) We further propose an over-propagation technique that can be used with any mark-and-sweep algorithm. The fact is that each triangle keeps one or more necessary linear distance fields, which may help determine the Voronoi bisectors.

3 OVERVIEW

We first consider a toy example with four sites specified on a 2D plane; See Fig. 2. For each site p_i, the distance field rooted at p_i can be visualized as an inverse cone, and the lower envelope of the four cones defines the multiple-source distance field as well as the two-dimensional VD; See Fig. 2(a). It can be seen that the multiple-source distance field has sharp ridges (whose projection induces the VD structure) where the distance change is far from being linear.

Now suppose that the input surface $\mathcal{S}$ is a planar or curved triangle surface. Let

$$D_i = \left\{ d_i^{(1)}, d_i^{(2)}, \cdots, d_i^{(j)}, \cdots, d_i^{(n)} \right\} \qquad (2)$$

be the i-th discrete distance field that keeps the distances at vertices, and n is the total number of vertices. By taking the change of a single-source distance field to be linear inside a triangle, the vector of D_i defines a piecewisely-linear approximation of the real distance field using n scalar values. The lower-envelope technique can be thus extended to polygonal surfaces by minimizing the group of piecewisely-linear geodesic distance fields, triangle by triangle; See Fig. 2(b). In fact, a linear distance field defined in a triangle can be understood as a half-plane over the base triangle. For each triangle, the lower envelope, determined by m sites, can be obtained by intersecting m half-planes.

Lifting [Fortune 1995] is a well-known technique that maps (x, y) to $(x, y, x^2 + y^2)$. Obviously, if we define a parabolic surface rooted at each site with squared distance, the lower envelope can also report the VD; See Fig. 2(c).

There are many research approaches [Moenning and Dodgson 2004] that suggest computing the surface-based VDs by running the multi-source geodesic distance algorithm that only keeps a minimum distance for each mesh vertex:

$$D_{\min} = \left\{ d_j^{\min} : \text{the distance from } v_j \text{ to the nearest site} \right\}_{j=1}^{n}.$$

But it is hard for them to extract an accurate VD from $D_{\min}$. As Fig. 2(d) shows, the traced bisectors are visually zigzag, due to the fact that $D_{\min}$, keeping only a minimum distance for each mesh vertex, is not informative enough to trace the VD structure.

In this paper, we propose to compute surface-based VDs based on two novel techniques. First, when inferring the lower envelope for a triangle, we simply replace the distance value at a vertex by the squared distance. The resulting VD is exact when $\mathcal{S}$ reduces to a planar surface; See Fig. 2(e), which is much different from the situation of Fig. 2(b). In Section 4.3, we prove the observation that squared-distance induces a natural extension of the VD from 2D to a curved surface. Second, it is obvious that computing a full distance field for every source site is time-consuming and unnecessary, so we propose an *over-propagation* distance field, where the distance field rooted at p_i is swept outward until it does not help determine the surface-based VD at all. The key strategy is to introduce a comparison rule between two triples (each triple defines a linear distance field in a triangle). It can be seen from Fig. 2(f) that the resulting diagram has no difference from Fig. 2(e), but the sweeping area is shrunk, greatly diminishing the computational cost. We shall elaborate on the two techniques in the next section.

Remark. As Fig. 2(e) shows, the assumption of squared-distance linearity coincidentally produces an exact VD when $\mathcal{S}$ reduces to a planar surface; See Section 4.3. But we must point out that the assumption does not apply to a curved surface. Despite this, the linearity assumption in terms of squared distance is still better than Euclidean distance; See Section 5. Besides, the linearity assumption holds only if the triangles are small enough because the geodesic distance field satisfies the Lipschitz continuity (note that the gradient norm cannot exceed 1).

4 ALGORITHM

To facilitate the explanation, we first introduce the over-propagation geodesic field in Section 4.1, and then justify how to lift the geodesic distance to the squared distance in Section 4.3.

4.1 Over-propagation

Essentially, the surface-based VD is formed due to the competition between different sites, i.e., a point $x \in \mathcal{S}$ belongs to p_i if and only if p_i can provide a shorter distance to x than the other sites. Suppose that we have an off-the-shelf mark-and-sweep distance field algorithm (e.g., the fast marching method or the window based

---

ALGORITHM 1: Using a typical mark-and-sweep algorithm to perform over-propagation, where the differences from the traditional multi-source sweep algorithm are highlighted with "★".

Input: A curved polygonal surface $\mathcal{S}$ and a set of source points $P = \{p_i\}_{i=1}^m$ on $\mathcal{S}$.

Output: Over-propagation distance field $D_{\min}$ rooted P.

foreach *triangle f* **do**
    Associate f with an empty half-plane list (★);
end

Initialize an empty priority queue Q for distance propagation;

foreach *source point $p \in \{p_i\}_{i=1}^m$* **do**
    Push a distance propagation event rooted at p to Q;
end

while Q *is not empty* **do**
    Take out the top-priority event *evt*;
    Extract the source point p encoded in *evt*;
      //When *evt* arrives at a mesh vertex v, we need to check each of v's incident faces;
    Extract the triangle f that *evt* arrives at;
    Check if *evt* can update the distance at one of the three vertices of f (★);
    if *p is a contributing source point for f* **then**
        Append p to the source-point list of f (★);
        Allow *evt* to generate new events of next generation in f and push them into Q;
    end
end

---

exact geodesic algorithms). There are two important aspects when using the distance solver to compute surface-based VDs: (1) how to maintain the sweeping of $\{D_i\}_{i=1}^m$ collaboratively and constrain each of them to sweep across an as-small-as-possible area, and (2) how to quickly fuse the distance fields to get the lower envelope that defines the surface-based VD.

Mark-and-sweep. There are many mark-and-sweep algorithms for computing a distance field or finding the shortest path on a polygonal surface $\mathcal{S}$, such as [Du et al. 2021a; Kimmel and Sethian 1998; Qin et al. 2017; Xin and Wang 2009]. Although being different in algorithm details, they share a similar algorithmic paradigm - propagating from near to far and prioritizing near-source distance propagation events, where each event contains a pair, i.e., the source point and the triangle, and also a value about the closest distance between them. The priority of events as well as the morphology of wavefronts is maintained by a priority queue, such that the events in the priority queue are processed according to the closest distances encoded by the events. When the source point of the current event cannot provide the closest distance to any vertex of the current triangle, the propagation process of the current source point on this triangle stops. The whole mark-and-sweep algorithm terminates when each vertex finds its nearest source point, resulting in a multi-source distance field. However, such a distance field is not
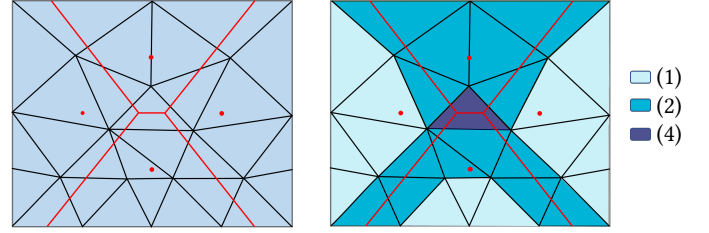

Fig. 3. Left: a planar mesh and the VD w.r.t. four sites. Right: for each triangle, we visualize how many distance fields (sources) really contribute to the triangle in a color-coding style.

informative enough to accurately trace the bisectors. Therefore, we keep all source points that contribute to each complete triangle (including its interior points), not just the vertices of the triangle. Details will be discussed below.

Filtering rule in over-propagation. A source point is not allowed to continue propagating across a triangle $f \triangleq v_1v_2v_3$, only if it is defeated by other source points in f. In other words, a source point p is said to be a *contributing* site to the triangle f, if p can provide the shortest distance for at least one point in f. Under the assumption that the distance field given by a single source is approximately linear in every triangle, p_i is defeated by p_j in f, only if

$$d_j^{(1)} < d_i^{(1)}, d_j^{(2)} < d_i^{(2)}, d_j^{(3)} < d_i^{(3)},$$

where $d_i^{(1)}, d_i^{(2)}, d_i^{(3)}$ are the three distances at v_1, v_2, v_3 given by p_i while $d_j^{(1)}, d_j^{(2)}, d_j^{(3)}$ are given by p_j. p is a contributing site to f if it cannot be defeated by any other source point in f's contributing-source list. As Algorithm 1 indicates, existing mark-and-sweep geodesic algorithm can be easily used for over-propagation by organizing all the propagation events into a prioritized queue. In Algorithm 1, the differences from the traditional multi-source sweep algorithm are highlighted with "★". In Fig. 3, we visualize distance triples (or equivalently source sites) that really contribute to the triangle at the end of the Algorithm 1.

Finding the lower envelope of half-planes. Suppose that $\triangle v_1v_2v_3$ is one of the triangles in the mesh. At the end of over-propagation, we assume that $p_1, p_2, \cdots, p_K \in P$ really contribute to $\triangle v_1v_2v_3$. Each site in P gives a distance triple that encodes a linear field in terms of geodesic distance. (Note that we will discuss the possibility of representing the linearity w.r.t. the squared distance.) Without loss of generality, we place $\triangle v_1v_2v_3$ on a 2D plane, by a rigid transform, such that the vertex v_j is located at (x_j, y_j), $j = 1, 2, 3$. p_i's distance field constrained in $\triangle v_1v_2v_3$ can be deemed to change linearly. We can use a half-plane π_i to define the linear approximation, where π_i passes through the following three points:

$$\left(x_1, y_1, d_g(p_i, v_1)\right), \left(x_2, y_2, d_g(p_i, v_2)\right), \left(x_3, y_3, d_g(p_i, v_3)\right),$$

where $d_g(p_i, v_j)$ means the distance between the source point p_i and the triangle vertex v_j.

The next task is to find the lower envelope of $\{\pi_i\}_{i=1}^K$. Our basic idea is to construct an infinite triangular prism with $\triangle v_1v_2v_3$ being the base and then incrementally cut the volume by $\{\pi_i\}_{i=1}^K$, like that achieved in [Du et al. 2021b]. We denote $d_i^{(1)} \triangleq d_g(p_i, v_1), d_i^{(2)} \triangleq$
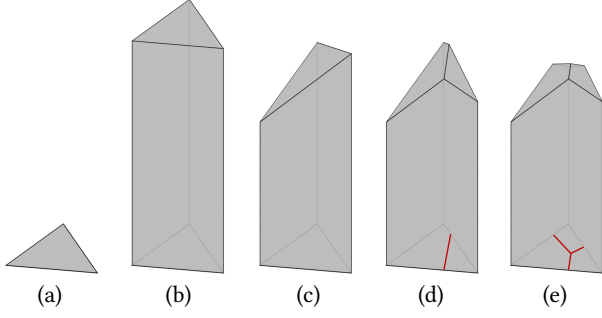
Fig. 4. We use a half-plane to encode the linear change of a distance field inside a triangle. During the mark-and-sweep process, the lower envelope over the triangle base can be obtained by incremental half-plane cutting. The VD restricted in the triangle can be traced accordingly.

$d_g(p_i, v_2)$, $d_i^{(3)} \triangleq d_g(p_i, v_3)$. Since each half-plane π_i cannot be vertical, we adopt the following representation form:

$$d = a_i x + b_i y + c_i,$$

where

$$\begin{pmatrix} a_i \\ b_i \\ c_i \end{pmatrix} = \begin{pmatrix} x_1 & y_1 & 1 \\ x_2 & y_2 & 1 \\ x_3 & y_3 & 1 \end{pmatrix}^{-1} \begin{pmatrix} d_i^{(1)} \\ d_i^{(2)} \\ d_i^{(3)} \end{pmatrix}.$$

Given a triple (x, y, d), the triple is on the upper side of π_i if

$$d \geq a_i x + b_i y + c_i,$$

and on the lower side if

$$d < a_i x + b_i y + c_i.$$

Fig. 4 shows the incremental plane cutting process. The VD restricted in the triangle can be reported at the same time.

Implementation. We give the pseudo-code of incremental half-plane cutting procedure in Algorithm 2. Each time when a new half-plane π comes, we will kill the existing vertices (of the up-to-date lower envelope) that are above π. Next, we identify those edges that pass through π. Suppose we are considering the edge $e = v_1 v_2$. If $\pi(v_1) = d_{v_1} - (a x_{v_1} + b y_{v_1} + c) > 0$ while $\pi(v_2) = d_{v_2} - (a x_{v_2} + b y_{v_2} + c) < 0$, we need to add a new vertex onto the up-to-date lower envelope:

$$v = \frac{\pi(v_1)}{\pi(v_1) - \pi(v_2)} v_2 - \frac{\pi(v_2)}{\pi(v_1) - \pi(v_2)} v_1.$$

The bounding edges of the envelope also need to be updated at the same time but the bounding facets do not. In addition, for consideration of run-time performance, we maintain the lower envelope for the triangle f only when the second triple (linear distance field) comes to f and the new triple has a chance to survive. Let K be the number of half-planes kept in the current triangle f. The number of vertices/edges/faces of the lower envelope is $O(K)$. The total time cost is bounded by $O(K^2)$.

4.2 Compatibility, consistence and connectedness

It seems that the past research lacks indicators to evaluate the quality of a surface-based VD. We propose three indicators to characterize if a surface-based VD is valid (see Fig. 5(a)). First, we hope that the

---

ALGORITHM 2: Incremental half-plane cutting

Input: $\triangle v_1 v_2 v_3$ and a set of half-planes $\{\pi_i\}_{i=1}^K$.
Output: Partition of $\triangle v_1 v_2 v_3$ based on the lower envelope
 of $\{\pi_i\}_{i=1}^K$.
Initialize a vertical prism truncated by $h = d_{\max}$ and
 $h = -d_{\max}$;
foreach $\pi \in \{\pi_i\}_{i=1}^K$ **do**
 Screen out vertices above π;
 Screen out useless edges;
 foreach *edge e crossing π* **do**
 Generate a new vertex;
 Update e's endpoint;
 end
end
Output the alive edges as the VD in $\triangle v_1 v_2 v_3$;

(a) An acceptable VD (b) Not compatible to 2D VD

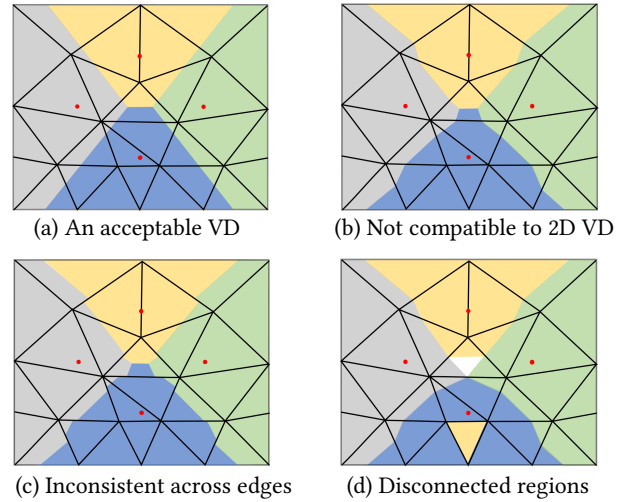(c) Inconsistent across edges (d) Disconnected regions

Fig. 5. For the applications, one hopes to obtain an acceptable VD that owns the following features: (1) it naturally reports the exact VD when the base surface reduces to a convex 2D domain, (2) the VD must be consistent across edges, i.e., passes through the same point of an edge for the two faces sharing the edge, and (3) no site is allowed to dominate multiple disconnected regions. In this figure, (a) shows an acceptable VD while (b,c,d) respectively show three situations that violate the three requirements.

resulting VD partition has no difference from the exact VD when the base surface becomes a convex 2D domain. If some surface VD algorithms report a partition in Fig. 5(b), it is not *compatible* with the 2D Voronoi diagram. Second, we hope that the extracted VD does not include breakpoints (see Fig. 5(c)) at mesh edges, i.e., for each mesh edge, the entry point of the VD must be identical to the exit point. We name this requirement *consistence*. Finally, we hope that each site dominates a connected region (may not be topologically equivalent to a disk), and all the regions form a covering of the whole surface. In this case, such surface VDs own *connectedness*. Fig. 5(d) shows an example where a site may dominate two or more regions (see the regions colored in yellow). Furthermore, the occurrence of
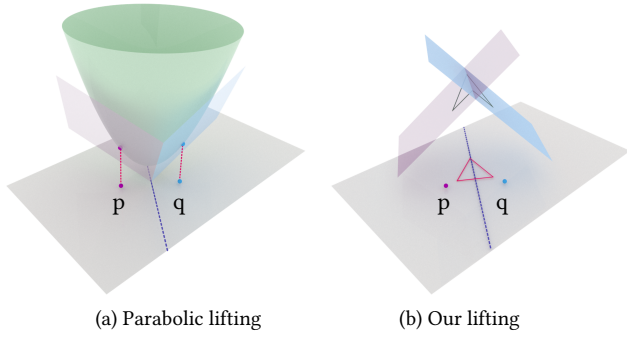
(a) Parabolic lifting   (b) Our lifting

Fig. 6. Two different lifting schemes. (a) The traditional lifting scheme lifts (x, y) to $(x, y, x^2 + y^2)$ that is located on a parabolic surface. It is well defined on a 2D plane but not easy to be extended to a curved surface. (b) Our lifting scheme lifts the three vertices of a triangle to $(x_1, y_1, d^2(p, v_1))$, $(x_2, y_2, d^2(p, v_2))$, $(x_3, y_3, d^2(p, v_3))$ for the site p while lifting the three vertices to $(x_1, y_1, d^2(q, v_1))$, $(x_2, y_2, d^2(q, v_2))$, $(x_3, y_3, d^2(q, v_3))$ for the site q.

an ownerless region also violates the requirement of connectedness; See the white region in Fig. 5(d).

Obviously, our over-propagation algorithm inherits the spirit of minimizing m continuous and piecewisely-linear distance fields. The resulting distance field, i.e., the lower envelope of the m distance fields, is also continuous, which guarantees the consistence. Besides, our algorithm is equipped with a mark-and-sweep distance solver, and thus each site detects its dominating area without destroying its connectivity, which guarantees the connectedness. In the following, we propose to use squared distance to define half-planes, which enables to further own the feature of compatibility.

4.3 Using squared distance to define half-planes

Definition 4.1. We assume that $\triangle v_1 v_2 v_3$ and a point $p(x_p, y_p)$ are in the xy-plane (p may be lying outside $\triangle v_1 v_2 v_3$), where the coordinates of the three vertices are $v_1(x_1, y_1), v_2(x_2, y_2), v_3(x_3, y_3)$. We define $\Pi^p_{v_1 v_2 v_3} \in \mathbb{R}^3$ to be the plane through the following three points:

$$(x_1, y_1, \|p - v_1\|^2), (x_2, y_2, \|p - v_2\|^2), (x_3, y_3, \|p - v_3\|^2),$$

and $z(x, y; \Pi^p_{v_1 v_2 v_3})$ to be the height at (x, y).

Definition 4.2. We assume that $\mathcal{P} : z = x^2 + y^2$ be the parabolic surface. Denote $\Pi^p_{\mathcal{P}}$ as the tangent plane at p's lifted point $(x_p, y_p, x_p^2 + y_p^2)$, i.e., $z = 2x_p x + 2y_p y - x_p^2 - y_p^2$. Similarly, we use $z(x, y; \Pi^p_{\mathcal{P}})$ to denote the height at (x, y).

As Fig. 6(a) shows, the traditional lifting scheme lifts (x, y) to $(x, y, x^2 + y^2)$ (a point on the parabolic surface $\mathcal{P} : z = x^2 + y^2$). Let p, q be the two sites respectively. The intersection line between the tangent plane $\Pi^p_{\mathcal{P}}$ at p's lifted point and that at q's lifted point, upon being projected onto the 2D plane, is exactly the perpendicular bisector of p and q. The traditional lifting scheme is well defined on a 2D plane but not easy to be extended to a curved surface.

In contrast, our lifting scheme is much different; See Fig. 6(b). Given a triangle $\triangle v_1 v_2 v_3$, the site p contributes to a lifted plane $\Pi^p_{v_1 v_2 v_3}$ passing through $(x_1, y_1, \|p - v_1\|^2), (x_2, y_2, \|p - v_2\|^2), (x_3, y_3, \|p -$

$v_3\|^2)$. Theorem 4.4 point out that our localized lifting scheme can also induce the exact 2D Voronoi diagram w.r.t. $\{p_i\}_{i=1}^m$, independent of the choice of $\triangle v_1 v_2 v_3$. In the following, we use $z(x, y; \Pi)$ to denote the height of Π at (x, y).

LEMMA 4.3. *For any non-degenerate triangle $\triangle v_1 v_2 v_3$ in the xy-plane, and any two different points $p(x_p, y_p), q(x_q, y_q)$ in the plane (may be outside $\triangle v_1 v_2 v_3$), we have*

$$z(x, y; \Pi^p_{v_1 v_2 v_3}) - z(x, y; \Pi^q_{v_1 v_2 v_3}) = z(x, y; \Pi^q_{\mathcal{P}}) - z(x, y; \Pi^p_{\mathcal{P}})$$

holds for any point (x, y).

PROOF. On the one hand,

$$z(x_1, y_1; \Pi^p_{v_1 v_2 v_3}) - z(x_1, y_1; \Pi^q_{v_1 v_2 v_3}) = \|p - v_1\|^2 - \|q - v_1\|^2.$$

On the other hand,

$$\begin{aligned} &z(x_1, y_1; \Pi^q_{\mathcal{P}}) - z(x_1, y_1; \Pi^p_{\mathcal{P}}) \\ =&2x_q x_1 + 2y_q y_1 - x_q^2 - y_q^2 - (2x_p x_1 + 2y_p y_1 - x_p^2 - y_p^2) \\ =&(x_p - x_1)^2 + (y_p - y_1)^2 - (x_q - x_1)^2 - (y_q - y_1)^2 \\ =&\|p - v_1\|^2 - \|q - v_1\|^2. \end{aligned} \tag{3}$$

By combining them, we have

$$z(x_1, y_1; \Pi^p_{v_1 v_2 v_3}) - z(x_1, y_1; \Pi^q_{v_1 v_2 v_3}) = z(x_1, y_1; \Pi^q_{\mathcal{P}}) - z(x_1, y_1; \Pi^p_{\mathcal{P}}),$$

which also holds for v_2 and v_3. Considering the assumption that v_1, v_2, v_3 are not co-linear and the fact that both

$$\left(z(x, y; \Pi^p_{v_1 v_2 v_3}) - z(x, y; \Pi^q_{v_1 v_2 v_3}) \right)$$

and

$$\left(z(x, y; \Pi^q_{\mathcal{P}}) - z(x, y; \Pi^p_{\mathcal{P}}) \right)$$

linearly depend on x and y, we finish the proof. □

Based on Lemma 4.3, it is easy to justify the triangle-based lifting scheme (see Fig. 6(b)) by the following theorem.

THEOREM 4.4. *Given $\triangle v_1 v_2 v_3$ in the xy-plane, as well as a set of sites $\{p_i\}_{i=1}^n$ on the plane (may be outside $\triangle v_1 v_2 v_3$), the configuration of the lower envelope of the following planes*

$$\Pi^{p_i}_{v_1 v_2 v_3}, \quad i = 1, 2, \cdots, n$$

defines the 2D Voronoi diagram w.r.t. $\{p_i\}_{i=1}^n$. Furthermore, the 2D Voronoi diagram is independent of the choice of $\triangle v_1 v_2 v_3$.

PROOF. Suppose that we have a parabolic surface $\mathcal{P} : z = x^2 + y^2$. It's well known that the upper envelope of

$$\Pi^{p_i}_{\mathcal{P}}, \quad i = 1, 2, \cdots, n$$

defines the Voronoi diagram. Based on Lemma 4.3, the inequality

$$z(x, y; \Pi^{p_i}_{\mathcal{P}}) - z(x, y; \Pi^{p_j}_{\mathcal{P}}) \geq 0$$

exactly implies

$$z(x, y; \Pi^{p_i}_{v_1 v_2 v_3}) - z(x, y; \Pi^{p_j}_{v_1 v_2 v_3}) \leq 0.$$

In this way, we verify the conclusion. □

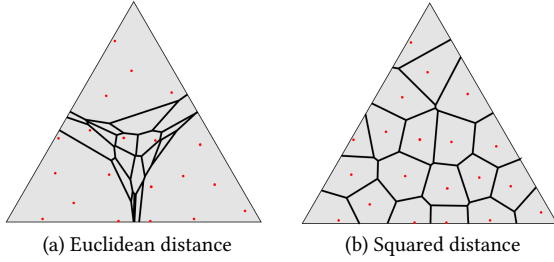(a) Euclidean distance   (b) Squared distance

Fig. 7. (a) Algorithm 1 cannot report an exact VD when the base surface degenerates to a convex 2D region, thus lacking the property of compatibility. (b) By using squared distance to define half-planes, the resulting VD is the same with the exact 2D Voronoi diagram, endowing Algorithm 1 with the property of compatibility and the ability of dealing with face-interior sites.

Remark on Theorem 4.4. In Section 4.1, we assume that every p-based geodesic distance field changes linearly in the triangle $\triangle v_1 v_2 v_3$. Lemma 4.3 indicates that it is better to assume that the squared distance, instead of the original geodesic distance or Euclidean distance, undergoes a linear change, i.e., the source point p_i defines a plane over $\triangle v_1 v_2 v_3$ that passes through

$$\left(x_1, y_1, \mathrm{d}_g^2(p_i, v_1)\right), \left(x_2, y_2, \mathrm{d}_g^2(p_i, v_2)\right), \left(x_3, y_3, \mathrm{d}_g^2(p_i, v_3)\right).$$

In this way, the property of "compatibility" can be guaranteed, without increasing the computational cost to Algorithm 1. The property of "compatibility" is very useful in practice. It enables Algorithm 1 to support face-interior sites; See Fig. 7.

We have finished decoupling the computation of surface-based VDs from the geodesic algorithms that are used to measure the distance between two points. By using different geodesic algorithms to measure the distance, we have at least three approaches for computing surface-based VDs.

- Exact geodesic Voronoi diagram (EGVD) that works with an exact geodesic algorithm;
- Approximate geodesic Voronoi diagram (AGVD) that works with the fast marching method;
- Euclidean distance based Voronoi diagram (EDBVD) that works with just Euclidean distance.

5 EVALUATION

5.1 Experimental setting

We implemented our algorithm in C++, which is independent of an off-the-shelf Voronoi/Delaunay solver, on the platform with a 2.8 GHz Intel Core i5-8400 CPU and Windows 10 operating system.

5.2 Comparison with the state of the arts

Fig. 8(a) shows a thin-sheet leaf model with 35K triangles. By specifying 100 sites on the surface, we compare with some known algorithms including RVD [Yan et al. 2009], LRVD [Yan et al. 2014], and diffusion diagram [Herholz et al. 2017]. As our approach supports various forms of geodesic distances, we respectively use exact geodesic distance (computed by the VTP geodesic algorithm [Qin et al. 2016]), approximate geodesic distance (computed by the fast marching method [Sethian 1999]), commute-time distance [Fouss

et al. 2007], biharmonic distance [Lipman et al. 2010], and even Euclidean distance as the distance solvers.

Among the existing algorithms, RVD is the most commonly used one in the computer graphics community, but the biggest disadvantage of RVD is that it may violate the "one site, one region" property, especially for those models with thin parts, resulting in many owner-less regions; See the highlighted regions in Fig. 8(c). Yan et al. [2014] proposed to improve the traditional RVD to localized RVD (LRVD) by enforcing a Dijkstra-sweep step. For a model with fair triangulation, if our algorithm takes Euclidean distance to drive the partition, the result is the same with LRVD because each curved bisector in LRVD or ours is obtained by intersecting the surface with a bisector plane between a pair of sites. But the Dijkstra-sweep along mesh edges may fail to report reliable neighboring relationship between sites on poorly triangulated surfaces; See [Wang et al. 2020] for detailed discussion. Our EDBVD, although it looks similar to LRVD, sweeps the surface from triangle to triangle while coordinating the propagation by the Euclidean distance, rather than the graph based distance reported by Dijkstra's algorithm. Therefore, EDBVD is independent of triangulation quality; See Fig. 9. Both LRVD and EDBVD have the "one site, one region" property. We observe that the results of LRVD and EDBVD may be different from the real GVD along the sharp edge of the geometry, due to the significant difference between Euclidean distance and geodesic distance.

To our knowledge, the diffusion diagram algorithm [Herholz et al. 2017] is also competitive in generating surface-based VDs; See Fig. 8(f). It takes the necessity of over-propagation into consideration but lacks a good strategy on reducing the propagation range. Besides, it is sensitive to the triangulation quality, and the resulting VD may be significantly different from the ground-truth when the base surface does not have a high triangle quality.

In contrast, our approach is flexible. It supports arbitrary distance solver as the plugin. Fig. 8(b,e,g,h,i) show some surface-based VDs given by different distance solvers. If we take the fast marching method as the plugin of our algorithm, the result is similar to Fig. 8(b) but not accurate. Commute-time distance (see Fig. 8(h)) or biharmonic distance (see Fig. 8(i)) is far from geodesic distance, thus leading to a VD much different from Fig. 8(b). Generally speaking, we recommend the fast marching method to drive the computation if the sites are very sparse, while using Euclidean distance directly if the sites are very dense. AGVD and EDBVD are enough for the most computer graphics applications. Fig. 10 shows a gallery of results computed by EDBVD. We also tested the exact geodesic distance driven GVD algorithms such as [Liu et al. 2017] and [Xu et al. 2014]. The resulting VDs are not significantly different from AGVD, but they are hundreds of times slower than our AGVD or thousands of times slower than our EDBVD. The detailed ratio depends on the mesh resolution and the number of sites.

5.3 Run-time performance

Fig. 11 shows a group of surface VD results on the Dragon model with 50K triangles, computed by EDBVD. By setting the number of sites to be 100, 300, 500, 700, and 900, the required timing costs are respectively 0.062 s, 0.094 s, 0.109 s, 0.125 s, and 0.130 s.

RVD, LRVD, and EDBVD are all based on Euclidean distance. Therefore, it is fair to compare the run-time performance among

(a) Input

(b) Ours+ExactGeodesic   (c) RVD   (d) LRVD   (e) Ours+Euclidean

(f) Diffusion Diagram   (g) Ours+FastMarching   (h) Ours+Commute-time   (i) Ours+Biharmonic
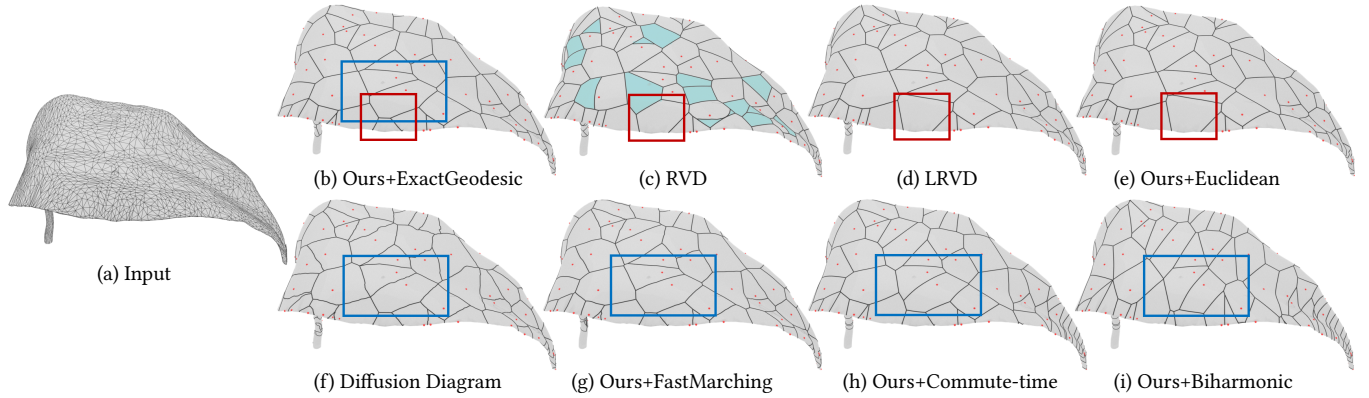
Fig. 8. Taking the Leaf model as the input (a), we visually compare the results produced by various approaches. We use the VTP algorithm to feed exact distances into our algorithm, yielding a high-quality surface VD (b). Both RVD (c) and LRVD (d) use the Euclidean distance to drive the surface partition, but RVD may produce ownerless regions (highlighted in light blue). If we takes Euclidean distance to drive the partition, the result (e) is the same as LRVD on this model (fair triangulation). Diffusion diagram (f) is inaccurate except that the input mesh is with a high triangulation quality. If we take the fast marching method (g) as the plugin, the results are similar to (b) but not accurate. Commute-time distance (h) or biharmonic distance (i) is far from geodesic distance, thus causing a VD to be very different from (b).
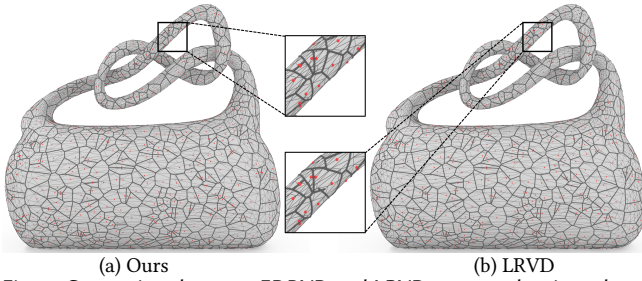

(a) Ours   (b) LRVD

Fig. 9. Comparison between EDBVD and LRVD on a poorly triangulated surface. Since the Dijkstra-sweep along mesh edges may fail to report reliable neighboring relationship between sites, LRVD may miss some bisectors but EDBVD cannot.

the three algorithms. We select four models for tests, i.e., 30K-face Vase, 30K-face Dolphin, 70K-face Bunny, and 100K-face Horse. By specifying various number of sites on these models, it shows that EDBVD outperforms RVD and LRVD in run-time, especially with an increasing number of sites. We also record some statistics of run-time in Table 1, where the best time data is highlighted in bold. Both Fig. 12 and Table 1 validate the efficiency of EDBVD.

Next, we come to analyze the time complexity of EDBVD. First, we assume that n and m are at the same order of magnitude, where m is the number of sites and n is the number of faces. We further assume that (1) the triangulation is dense and fine, (2) each site dominates only several triangles, and (3) the number of sites in a triangle can be bounded by $O(1)$. On the one hand, the time cost for conducting the propagation of each site is $O(1)$, and thus the total timing cost spent in distance propagation can be bounded by $O(m)$. Additionally, each triangle receives a limited number of distance triples, generally between 1 to 3, if no serious coincidence occurs. The total timing cost spent in half-plane cutting can be bounded by $O(n)$. Therefore, the average time complexity of our EDBVD algorithm is $O(m + n)$. If $m \ll n$, then the total timing cost spent in distance propagation may amount to $O(n \log n)$. In this

Table 1. Performance statistics of RVD, LRVD and our EDBVD (in seconds), where the best run-time performance is highlighted in bold.

Model	Faces	Method	Number of sampling points				
			4K	8K	12K	16K	20K
Vase	30K	RVD	0.126	0.219	0.297	0.422	0.515
		LRVD	0.157	0.203	0.235	0.297	0.328
		EDBVD(Ours)	**0.125**	**0.187**	**0.219**	**0.250**	**0.281**
Bunny	70K	RVD	**0.203**	0.297	0.406	0.501	0.610
		LRVD	0.313	0.391	0.485	0.547	0.625
		EDBVD(Ours)	0.219	**0.281**	**0.361**	**0.407**	**0.453**
Horse	100K	RVD	**0.253**	**0.344**	0.485	0.593	0.718
		LRVD	0.406	0.516	0.625	0.734	0.863
		EDBVD(Ours)	0.281	0.359	**0.422**	**0.547**	**0.550**
Dolphin	180K	RVD	**0.341**	**0.465**	0.654	0.801	0.942
		LRVD	0.619	0.781	0.957	1.070	1.250
		EDBVD(Ours)	0.401	0.501	**0.583**	**0.660**	**0.742**
Kitten	270K	RVD	**0.593**	0.756	0.945	1.323	1.667
		LRVD	0.672	0.922	1.141	1.391	1.656
		EDBVD(Ours)	0.609	**0.641**	**0.781**	**0.843**	**0.921**

case, the average time complexity of EDBVD becomes $O(n \log n)$. If $m \gg n$, instead, then the propagation cost is $O(m)$ (in the average case) and the cost of half-plane cutting amounts to $O(n \times (\frac{m}{n})^2)$ (see Section 4.1), making the total time complexity $O(\frac{m^2}{n})$, which indicates that a highly efficient half-plane cutting solver is necessary when m is large.

Finally, we must point out that if a different distance solver is used, the time complexity must be different. We come to analyze the average time complexity under the assumption of fair triangulation and uniform distribution of sites. Suppose that we are using the fast marching method, running in time $O(n \log n)$, as the distance solver. If $m \ll n$, the average time complexity climbs to $O(n \log n)$. For $m = O(n)$ and $m \gg n$, the time complexity remains unchanged, i.e., $O(m + n)$ for $m = O(n)$ and $O(\frac{m^2}{n})$ for $m \gg n$.

Fig. 10. More surface VDs produced by our EDBVD.

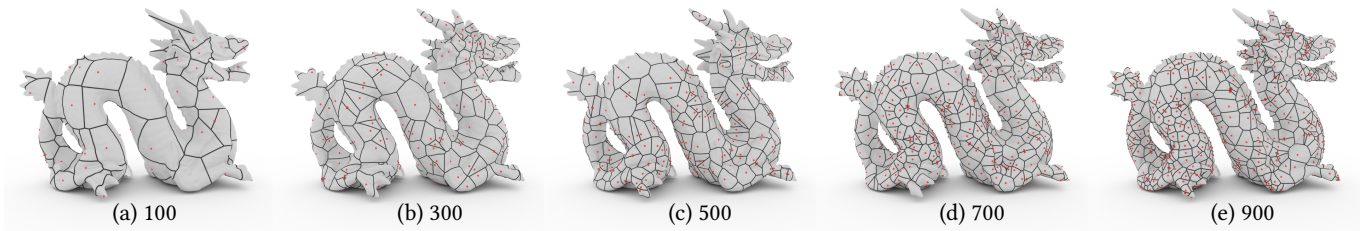| (a) 100 | (b) 300 | (c) 500 | (d) 700 | (e) 900 |

Fig. 11. Test EDBVD on the Dragon model by specifying various number of sites, where the base surface is with 50K triangles.
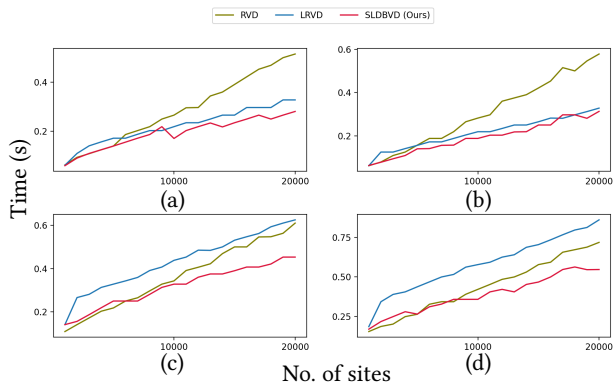

Fig. 12. Run-time performance comparison among RVD, LRVD and our EDBVD. (a) Vase: 30K faces. (b) Dolphin: 30K faces. (c) Bunny: 70K faces. (d) Horse: 100K faces.

Fig. 13. Surface VDs with feature-line constraints.

5.4 Extendability

Our algorithm is able to deal with various variants of surface-based partition problems including breakline constraints, face-interior point sites, curve-type sites, density-equipped surfaces, and even surface restricted power diagram.

Surface VDs with breakline constraints. There are many scenarios where one inputs a set of curves to constrain the computation of VDs [Tournois et al. 2010]. For example, there is a requirement in mesh generation that VD cells are not allowed to extend across feature lines. In fact, our algorithm can solve the stumbling problem easily. Imagining that there is a linear distance field that defines a half-plane π over the triangle f, and f contains a line-segment breakline. We only need to use the vertical plane passing through
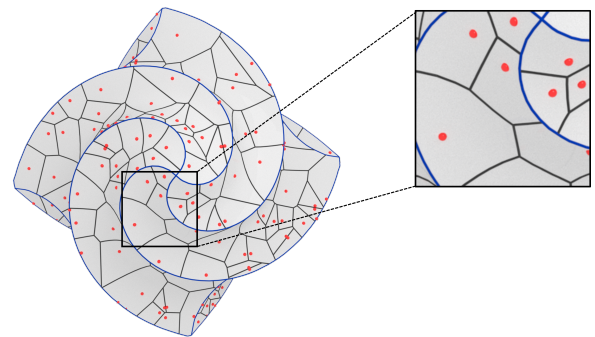
the line-segment breakline as a barrier, and prevent π crossing the vertical plane. Fig. 13 shows a model with 16K faces and there are 300 sites on the surface. The feature lines are colored in blue. By taking these feature lines as breaklines, our algorithm is able to preserve the feature lines in computing the surface VD. For this example, the total computational time is just 62ms.

Restricted power diagram. Our algorithm can be used to compute surface restricted power diagrams; See Fig. 14. For each vertex v, we keep the squared distance in our implementation, i.e., $\|v-p\|^2$, where p is a site. If p has a weight of w, then according to the definition of power diagram, the weighted distance to v given by p becomes $\|v-p\|^2 - w$. The linear distance field in the triangle $\triangle v_1 v_2 v_3$ is then given by

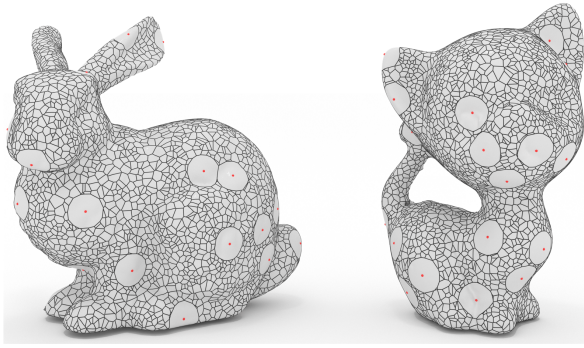$$\|v_1 - p\|^2 - w, \|v_2 - p\|^2 - w, \|v_3 - p\|^2 - w.$$

Fig. 14. Surface restricted power diagram.

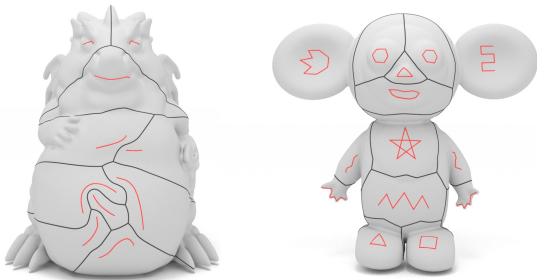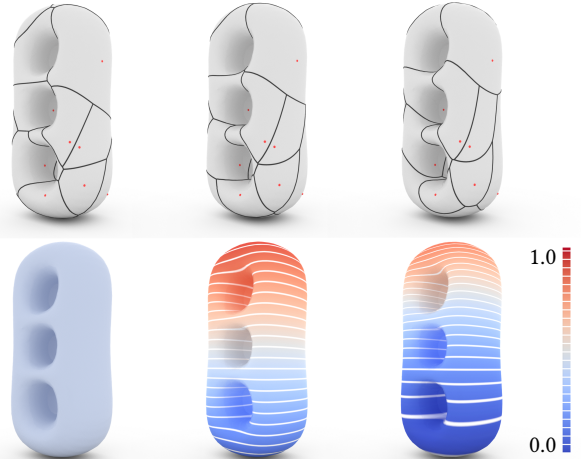Fig. 15. Our algorithm supports curve-type sites.

(a) Constant density   (b) Linear density   (c) Non-linear density

Fig. 16. Surface VDs on the genus-3 Torus model with different density settings. Our algorithm supports the input surface equipped with a non-uniform density field.

(a) Original mesh   (b) Remesh with 1K vertices

(c) Remesh with 4K vertices   (d) Remesh with 6K vertices

Fig. 17. We validate the numerical robustness of EDBVD in remeshing. By placing 1K, 1.1K, 1.2K, · · · , 6K blue-noise sites, respectively, our implementation does not encounter a failure case.

In this way, the bisectors of restricted power diagram can be still computed by intersecting half-planes. For the two examples shown in Fig. 14, i.e., 70K-face Bunny with 6K sites and 270K-face Kitten with 5K sites, the total computational costs are 0.234 s and 0.633 s, respectively.

Curve-type sites. The VD bisectors w.r.t. curve-type sites are more curved than the situation of point-type sites, making the computation of VDs very challenging. Xu et al. [2014] proposed a local Voronoi diagram (LVD) to deal with curve-type generators, which is mainly based on the technique of additively weighted Voronoi diagram and requires a high computational cost. For a point-type site p, we keep the squared distance, at a mesh vertex v, in our implementation, i.e., $\|v - p\|^2$. If the point-type sites become curve-type sites, it is enough to replace the point-to-point distance with the point-to-curve distance. The simple trick produces a good approximation to the VD of the curve-type sites; See Fig. 15. We must point out that RVD includes a step of calling an off-the-shelf Delaunay triangulation solver, and thus cannot deal with curve-type sites.

VD on a surface with density field. In many digital geometry processing applications, the surface is equipped with a density field. In the default setting, the density field is identity. But the density field may also be the local-feature-size function, shape diameter function, mean curvature, or a kind of important field. A basic requirement is to distribute sample points to adapt to the given density field. To our best knowledge, there is no density-aware Voronoi/Delaunay solver available yet, limiting the use of RVD in handling the density equipped surfaces.

Under the assumption that the density function can be extended from the surface to 3D, i.e., $\rho = \rho(x, y, z)$, our EDBVD can easily address the challenge. Let v be a mesh vertex and p be one of the source points. It suffices to compute the distance as

$$d_\rho(v, p) = d(v, p) \int_0^1 \rho(t)\mathrm{d}t,$$

where $d(v, p)$ is the Euclidean distance between v and p, $\rho(t)$ is the density value at the point $(1 - t)v + tp$ (a point on the line segment $\overline{vp}$), and $d_\rho(v, p)$ is the density-equipped distance. Based on this observation, we can use the squared density-equipped distance to define half-planes, yielding density-equipped VDs. In Fig. 16, we

show a genus-3 Torus model with 30K faces, as well as the VDs for three different density settings. It can be seen that the bisectors tend to move toward the regions with larger density. Note that it costs only 35 ms to compute a density-equipped VD on this model.

Validation on numerical robustness. To validate our algorithm in numerical robustness, we run EDBVD to accomplish the remeshing task by placing a various number of sites, which only needs to add a step of extracting the dual of the VD. We take the Fertility model with 36K triangles (see Figure 17(a)) as the base surface and place 1K, 1.1K, 1.2K, $\cdots$, 6K sites following the blue-noise distribution, respectively. No failure case occurs, which validates the numerical robustness of our algorithm. Figure 17(b,c,d) show the remeshed results for 1K, 4K, and 6K sites, respectively. The timing costs for the three results are 0.082 s, 0.152 s, and 0.189 s, respectively.

6 CONCLUSION, LIMITATIONS AND FURTHER WORK

In this paper, we propose a powerful algorithm, named SurfaceVoronoi, for computing surface-based Voronoi diagrams. The distinguished features of SurfaceVoronoi are two-fold: (1) using the over-propagation mechanism to keep one or more necessary distance triples, for each triangle, that may help determine the Voronoi bisectors, and (2) using the squared distance to define the linear change of distance in a triangle, which is a provably meaningful extension from the traditional 2D Voronoi diagram to curved surfaces. SurfaceVoronoi has several nice features. First, it can work with an arbitrary geodesic algorithm. Especially, our algorithm, when driven by Euclidean distance, is able to deal with thin-sheet models and runs faster than RVD and LRVD. Second, it does not need an existing Voronoi/Delaunay solver and is flexible enough to deal with various VD problems including breakline constraints, face-interior point sites, curve-type sites, density-equipped surfaces, and even surface restricted power diagram.

Our algorithm, still needs to be improved. First, the plane cutting operation is un-optimized and can be accelerated. Second, if a time-consuming distance solver is used (e.g., an exact geodesic algorithm that is empirically $O(n\sqrt{n})$), the overall time cost is huge especially when the base surface contains a large number of triangles but just a few sites on the surface. Last but not least, numerical issues may occur when very long-and-thin triangles exist. In the future, we will explore the possibility of speeding up the computation and extending SurfaceVoronoi to broken meshes.

REFERENCES

P. Alliez, Éric Colin de Verdière, O. Devillers, and M. Isenburg. 2005. Centroidal Voronoi diagrams for isotropic surface remeshing. *Graph. Model.* 67 (2005), 204–231.

Jie Du, Ying He, Zheng Fang, Wenlong Meng, and Shiqing Xin. 2021a. On the Vertex-oriented Triangle Propagation (VTP) Algorithm: Parallelization and Approximation. *Computer-Aided Design* 130 (2021), 102943.

Xingyi Du, Qingnan Zhou, Nathan Carr, and Tao Ju. 2021b. Boundary-Sampled Halfspaces: A New Representation for Constructive Solid Modeling. *ACM Trans. Graph.* 40, 4 (2021).

Steven Fortune. 1987. A sweepline algorithm for Voronoi diagrams. *Algorithmica* 2, 1-4 (1987), 153.

Steven Fortune. 1995. Voronoi diagrams and Delaunay triangulations. In *Computing in Euclidean geometry*. World Scientific, 225–265.

Francois Fouss, Alain Pirotte, Jean-michel Renders, and Marco Saerens. 2007. Random-Walk Computation of Similarities between Nodes of a Graph with Application to Collaborative Recommendation. *IEEE Transactions on Knowledge and Data Engineering* 19, 3 (2007), 355–369.

Peter Giblin and Benjamin B Kimia. 2004. A formal classification of 3D medial axis points and their local geometry. *IEEE Transactions on Pattern Analysis and Machine Intelligence* 26, 2 (2004), 238–251.

Peter J Green and Robin Sibson. 1978. Computing Dirichlet tessellations in the plane. *The computer journal* 21, 2 (1978), 168–173.

Philipp Herholz, Felix Haase, and Marc Alexa. 2017. Diffusion Diagrams: Voronoi Cells and Centroids from Diffusion. *Computer Graphics Forum* 36, 2 (2017), 163–175.

Marc Khoury and Jonathan Richard Shewchuk. 2016. Fixed Points of the Restricted Delaunay Triangulation Operator. In *32nd International Symposium on Computational Geometry (SoCG 2016)*. 47:1–47:15.

Ron Kimmel and James A Sethian. 1998. Computing geodesic paths on manifolds. *Proceedings of the national academy of Sciences* 95, 15 (1998), 8431–8435.

Bruno Lévy and Yang Liu. 2010. L_p Centroidal Voronoi Tessellation and its applications. *ACM Transactions on Graphics (TOG)* 29, 4 (2010), 1–11.

Yaron Lipman, Raif M. Rustamov, and Thomas A. Funkhouser. 2010. Biharmonic Distance. *ACM Trans. Graph.* 29, 3 (2010).

Yong-Jin Liu, Zhanqing Chen, and Kai Tang. 2010. Construction of iso-contours, bisectors, and Voronoi diagrams on triangulated surfaces. *IEEE Transactions on Pattern Analysis and Machine Intelligence* 33, 8 (2010), 1502–1517.

Yong-Jin Liu, Dian Fan, Chun-Xu Xu, and Ying He. 2017. Constructing intrinsic Delaunay triangulations from the dual of geodesic Voronoi diagrams. *ACM Transactions on Graphics (TOG)* 36, 2 (2017), 1–15.

Joseph SB Mitchell, David M Mount, and Christos H Papadimitriou. 1987. The discrete geodesic problem. *SIAM J. Comput.* 16, 4 (1987), 647–668.

Carsten Moenning and Neil A Dodgson. 2004. Intrinsic point cloud simplification. *Proc. 14th GrahiCon* 14 (2004), 23.

Yipeng Qin, Xiaoguang Han, Hongchuan Yu, Yizhou Yu, and Jianjun Zhang. 2016. Fast and exact discrete geodesic computation based on triangle-oriented wavefront propagation. *ACM Transactions on Graphics (TOG)* 35, 4 (2016), 1–13.

Yipeng Qin, Hongchuan Yu, and Jianjun Zhang. 2017. Fast and Memory-Efficient Voronoi Diagram Construction on Triangle Meshes. *Computer Graphics Forum* 36, 5, 93–104.

Guodong Rong, Miao Jin, and Xiaohu Guo. 2010. Hyperbolic Centroidal Voronoi Tessellation. In *Proceedings of the 14th ACM Symposium on Solid and Physical Modeling* (Haifa, Israel). ACM, NY, USA, 117–126.

Marjorie Senechal. 1993. Spatial tessellations: Concepts and applications of Voronoi diagrams. *Science* 260, 5111 (1993), 1170–1173.

J. A. Sethian. 1999. Fast Marching Methods. *SIAM Rev.* 41, 2 (1999), 199–235.

Michael Ian Shamos and Dan Hoey. 1975. Closest-point problems. In *16th Annual Symposium on Foundations of Computer Science*. IEEE, 151–162.

Jane Tournois, Pierre Alliez, and Olivier Devillers. 2010. 2D centroidal Voronoi tessellations with constraints. *Numerical Mathematics: Theory, Methods and Applications* 3, 2 (2010), 212–222.

Pengfei Wang, Shiqing Xin, Changhe Tu, Dongming Yan, Yuanfeng Zhou, and Caiming Zhang. 2020. Robustly computing restricted Voronoi diagrams (RVD) on thin-plate models. *Computer Aided Geometric Design* (2020), 101848.

Xiaoning Wang, Xiang Ying, Yong-Jin Liu, Shi-Qing Xin, Wenping Wang, Xianfeng Gu, Wolfgang Mueller-Wittig, and Ying He. 2015. Intrinsic computation of centroidal Voronoi tessellation (CVT) on meshes. *Computer-Aided Design* 58 (2015), 51–61.

Shi-Qing Xin and Guo-Jin Wang. 2009. Improving Chen and Han's algorithm on the discrete geodesic problem. *ACM Transactions on Graphics (TOG)* 28, 4 (2009), 1–8.

Chunxu Xu, Yong-Jin Liu, Qian Sun, Jinyan Li, and Ying He. 2014. Polyline-sourced Geodesic Voronoi Diagrams on Triangle Meshes. *Computer Graphics Forum* 33, 7, 161–170.

Dong-Ming Yan, Guanbo Bao, Xiaopeng Zhang, and Peter Wonka. 2014. Low-resolution remeshing using the localized restricted Voronoi diagram. *IEEE transactions on visualization and computer graphics* 20, 10 (2014), 1418–1427.

Dong-Ming Yan, Bruno Lévy, Yang Liu, Feng Sun, and Wenping Wang. 2009. Isotropic remeshing with fast and exact computation of restricted Voronoi diagram. *Computer graphics forum* 28, 5, 1445–1454.

Dong-Ming Yan, Wenping Wang, Bruno Lévy, and Yang Liu. 2013. Efficient computation of clipped Voronoi diagram for mesh generation. *Computer-Aided Design* 45, 4 (2013), 843–852.

Rhaleb Zayer, Daniel Mlakar, Markus Steinberger, and Hans-Peter Seidel. 2018. Layered Fields for Natural Tessellations on Surfaces. *ACM Trans. Graph.* 37, 6 (2018).